Investigation of the dynamics of 1-octene adsorption at 293 K in a ZSM-5 catalyst by inelastic and quasielastic neutron scattering

Alexander P. Hawkins, Alexander J. O'Malley, Andrea Zachariou, Paul Collier, Russell A. Ewings, Ian P. Silverwood, Russell F. Howe, Stewart F. Parker and David Lennon

Published version information

Citation: AP Hawkins et al. "Investigation of the dynamics of 1-octene adsorption at 293 K in a ZSM-5 catalyst by inelastic and quasielastic neutron scattering." Journal of Physical Chemistry C, vol. 123, no. 1 (2018): 417-425.

DOI: 10.1021/acs.jpcc.8b08420

Investigation of the dynamics of 1-octene adsorption at 293 K in a ZSM-5 catalyst by inelastic and quasielastic neutron scattering

Alexander P. Hawkins,[ab] Alexander J. O'Malley,[bc] Andrea Zachariou,[ab] Paul Collier,[d] Russell A. Ewings,[e] Ian P. Silverwood,[e] Russell F. Howe,[f] Stewart F. Parker,[be] and David Lennon*[ab]

[a] School of Chemistry, Joseph Black Building, University of Glasgow, Glasgow G12 8QQ, UK

[b] UK Catalysis Hub, Research Complex at Harwell, STFC Rutherford Appleton Laboratory, Chilton, Oxon OX11 0FA, UK

[c] Cardiff Catalysis Institute, School of Chemistry, Cardiff University, Main Building, Cardiff, CF10 3AT, UK.

[d] Johnson Matthey Technology Centre, Blounts Court, Sonning Common, Reading RG4 9NH, UK

[e] ISIS Facility, STFC Rutherford Appleton Laboratory, Chilton, Oxon OX11 0QX, UK

[f] Department of Chemistry, University of Aberdeen, Aberdeen, AB24 3UE, UK

Abstract: The properties of 1-octene adsorbed in zeolite ZSM-5 at 293 K are studied by means of inelastic and quasielastic neutron scattering (INS and QENS) in order to investigate interactions relevant to the zeolite solid acid catalysis of fluidised catalytic cracking reactions. The INS spectrum is compared to that recorded for the solid alkene and reveals significant changes of bonding on adsorption at ambient temperatures; the changes are attributed to the oligomerization of the adsorbed 1-octene to form a medium chain *n*-alkane or *n*-alkane cation. QENS analysis shows that these oligomers are immobilised within the zeolite pore structure but a temperature-dependant fraction is able to rotate around their long axis within the pore channels.

1 Introduction

ZSM-5 is an MFI-structured zeolite which is widely used in commercial Fluidised Catalytic Cracking (FCC) operations as an additive catalyst in combination with conventional Zeolite Y.[1] When first commercialised, ZSM-5 was used primarily as an octane-boosting isomerisation additive but more recent interest is due to its ability to enhance the yield of light olefins in the FCC product stream by selective cracking of gasoline range *n*-olefins.[1-3] Liquid Petroleum Gas-range olefins are important chemical precursors for both polymer and industrial chemical production and, while demand for them is increasing globally, production of hydrocarbons in this class, other than ethene, actually decreased from 2005-2010 and continues to be lower than demand due to changes in the international petrochemical supply chain.[4] Increasing olefin yields from FCC cracking of gasoline through more selective catalysts is a technology well placed to fill this gap in the market.[2, 4-6]

The selectivity of ZSM-5 towards light olefin production is attributed to a shape-selective effect due to the confined volume within the zeolite pore structure. Cracking proceeds *via* the protonation of the C=C bond by a zeolite Brønsted site, followed by β-scission and isomerisation to form shorter chain alkenes.[7] The confined volume of the 2.75 Å ZSM-5 pore radius means that this reaction occurs through solely monomolecular mechanisms and prevents the oligomerization of larger molecules or isomerisation to branched structures that can occur in less confining structures like zeolite Y (pore radius 3.7 Å).[8] Branched olefin fractions of the feedstock are similarly excluded from the cracking reaction by their inability to access the pore interior and its acid sites.[2, 7, 9] The catalytic activity of the zeolite is also affected by its acidity; it is

noted that in commercial use the catalyst undergoes steaming which reduces the overall Brønsted acidity, which in turn results in the commercial catalyst selectively cracking olefins which can still take place with the lower acidic strength, while the untreated catalyst is capable of cracking both olefin and paraffin substrates.[10] The steaming process is also found to result in structural changes in the zeolite due to de-alumination and the generation of extra-framework alumina sites.[11]

Due to the influence of these structural factors, understanding how cracking substrate species interact with, and diffuse within, the zeolite structure are important factors in understanding the zeolite's catalytic activity. Neutron spectroscopy techniques represent a particularly powerful tool for the study of these interactions. The use of quasielastic neutron scattering (QENS) to study the diffusion of hydrocarbons in zeolites is well established across a variety of hydrocarbon and zeolite catalyst systems.[12-16] QENS techniques cover a range of timescales similar to that observed for hydrocarbon diffusion in zeolites, have high sensitivity to hydrocarbon sorbate species due to the scattering properties of hydrogen, and are amenable to comparison with results obtained from molecular dynamics simulations.[14]

For study of the zeolite-hydrocarbon interactions, conventional spectroscopic techniques have historically been hindered by the location of the sites of interest within the zeolite pore structure and the presence of strong zeolite framework vibrations in the infrared below 1500 cm^{-1} obscuring vibrational bands of interest. Raman spectroscopy is hindered by sample fluorescence. NMR studies have achieved some success, including the suggestion that *n*-olefins adsorbed in ZSM-5 may be present as carbocations even at temperatures where β-scission and cracking does not occur.[17]

Inelastic neutron scattering (INS) can provide information on the vibrational motions in a zeolite catalyst while sidestepping the issue of framework masking due to the exceptionally high inelastic incoherent scattering cross section of hydrogen, meaning that modes of relevance to the catalyst-hydrocarbon interactions dominate the spectrum.[18] The ability of INS to detect hydrocarbon changes in zeolite catalysed systems has been recently proven for an investigation of the Methanol-to-Hydrocarbons reaction,[19-20] and the technique appears equally suitable for application to FCC connected reaction systems.

Given the potential of INS to provide additional insight into the catalyst-hydrocarbon reactions in FCC systems, we report here the results of a combined INS and QENS study of the interactions of 1-octene with an unsteamed ZSM-5 catalyst at 293 K. 1-octene was chosen as a representative compound for the type of gasoline-range olefin which forms the reactive fraction in FCC feedstocks over ZSM-5. Investigations were performed with the 1-octene at low temperatures compared to typical FCC reaction conditions in order to establish the pre-reaction behaviour of the reactant species. The ability of ZSM-5 to oligomerize short-chain olefins at low temperatures is well reported, however, 1-octene lies within the range of olefin chain lengths which are generally reported as terminal species for this reaction at temperatures < 473 K.[17, 21-22] The use of INS to provide insight into the interactions of an olefin with a cracking catalyst is a novel application of this technique. As mentioned above, the industrial operation utilises a steamed ZSM-5 catalyst. However, in order to understand the surface chemistry of the ZSM-5/1-octene reaction system, this study will concentrate on how the adsorbate reacts with an activated ZSM-5 sample at relatively low temperatures with the sample experiencing no prior steam treatment. Against this background,

future studies can then examine steamed ZSM-5 samples with moderated Brønsted acidity that more closely connects with the industrial scenario.

2 Experimental

The ZSM-5 zeolite used was a commercial catalyst grade supplied in powder form by Johnson Matthey. From this point on it will be referred to as *the* catalyst. Previous studies using the same zeolite batch have established it as possessing a Si:Al ratio of ~30.[20] The catalyst as supplied was heated in static air at 10 K min^{-1} to 773 K and held for 12 hours to remove residual template material through calcination. BET analysis was performed on the calcined material to establish the pore surface area, yielding an average value of 370 m^2g^{-1}.

2.1 Inelastic Neutron Scattering

A quantity of calcined catalyst suitable for INS measurements (10.78g) was loaded into an Inconel reactor of 35mm internal diameter and mounted on a gas handling apparatus at the ISIS Facility which is described in detail elsewhere.[23] This was heated at 10 K min^{-1} to 623 K under a continuous flow of helium (1000 sccm, BOC, 99.999%) and held for 3 hours to dry the catalyst. The reactor was allowed to cool under He flow to ambient temperature and isolated for transfer to an argon filled glove box (MBraun UniLab MB-20-G, [H_2O] < 1 ppm, [O2] < 1 ppm) where the dried catalyst was loaded into an aluminium INS sample can equipped with gas handling fittings. The design of this can is similar to that of the steel sample environment previously reported by Warringham, et al.[23] with the exception of the replacement of the copper CF flange seals with compressed indium wire gaskets; the sample volume exposed to the neutron beam

remains a flat 50 × 50 × 10 mm plate. The sample was moved to the INS spectrometers to acquire background vibrational spectra of the clean, activated zeolite, as described below. Following background acquisition the catalyst was dosed *ex situ* with 1-octene using flowing helium at 200 sccm passed through a bubbler arrangement at 293 K; gravimetric analysis indicated a final 1-octene loading of 1.03×10^{-3} mol g^{-1}_{cat}, equating to 5.96 octene molecules per ZSM-5 unit cell. The dosed sample was returned to the spectrometers and the spectra of the loaded catalyst taken. Finally, the spectra of a 3.81g sample of 1-octene was taken for comparison purposes using a flat, indium-sealed aluminium sample can optimised for the measurement of pure liquids with a sample volume of 20 × 30 × 1 mm.

All INS measurements were performed at ≤30 K using two INS spectrometers. Initial measurements were performed on MAPS, a direct-geometry inelastic spectrometer which provides access to the C-H and O-H stretching region of the vibrational spectrum.[18] All spectra were recorded using the high resolution A-chopper package at incident energies of 5244 and 2017 cm^{-1}, with frequencies of 600 and 400 Hz respectively. The MAPS spectra reproduced in
Figure 1 were integrated over a momentum transfer (Q) range of $0 \leq Q \leq 10$ $Å^{-1}$ to eliminate overtone contributions present at higher Q values. For greater spectral resolution below 1200 cm^{-1} , all samples were also measured on the indirect geometry spectrometer TOSCA.[24] Time-of-flight data for both sets of measurements were reduced to spectra using the Mantid software package,[25] while integration of the MAPS data made use of the analysis tool MSlice.[26]

2.2 Quasielastic Neutron Scattering

QENS measurements are performed with smaller sample sizes in order to avoid multiple scattering; 2.27g of calcined ZSM-5 was loaded into a 2 mm annular niobium sample can equipped with gas handling fittings and copper-gasketed CF seals, the design of

which has been previously described by Silverwood and Sakai[27]. This was mounted on the gas handling apparatus and dried in the same manner as the INS sample. Once cool, the sample was transferred directly to the OSIRIS low-energy backscattering spectrometer to record background spectra. All measurements were performed using the (002) reflection of the graphite analyser crystal which offers an energy resolution of 25.4 μeV and a momentum transfer range of 0.18-1.8 $Å^{-1}$.[28] Spectra were recorded at 6 K to provide an instrument resolution function and at 273, 323 and 373 K. The sample was allowed to cool to room temperature then dosed *ex situ* with 1.06×10^{-3} mol g^{-1}_{cat}, equating to 6.49 1-octene molecules per unit cell, using the method described above. The dosed sample was returned to OSIRIS and a set of spectra recorded at identical conditions to the background measurement. The background spectra previously recorded were subtracted from these dosed spectra to remove the contributions to the scattering function from coherent scattering from the zeolite framework, leaving only the contributions from the adsorbed hydrocarbon: this simplifies the process of deriving an accurate fit for the quasielastic data. Time-of-flight datasets were again reduced using Mantid while baseline subtraction, peak fitting and other data analysis operations were carried out using the data analysis software suite DAVE.[29]

3 Results and Discussion

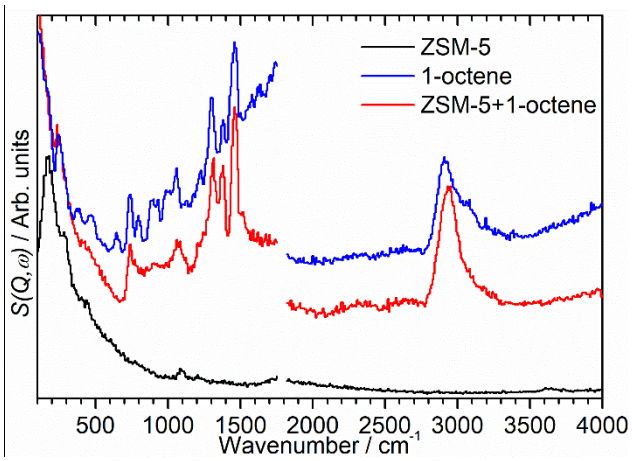

Figure 1: INS spectra of clean ZSM-5 (black), pure 1-octene (blue) and 1-octene in ZSM-5 (red) recorded on the MAPS spectrometer at incident energies of 2017 (*left*) and 5244 (*right*) cm^{-1}. Spectra integrated over the momentum transfer range $0 \leq Q \leq 10$ $Å^{-1}$. Intensities are scaled to correct for the different sample sizes and the spectra are offset in *y*-axis for clarity.

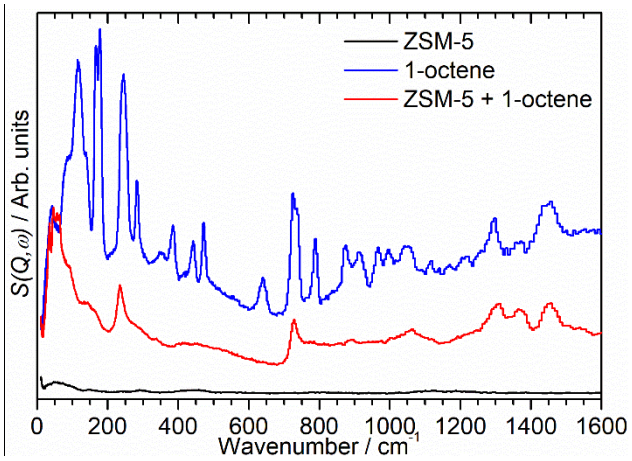

Figure 2: 0-1600 cm^{-1} region of the TOSCA INS spectra for clean ZSM-5 (black), pure 1-octene (blue) and 1-octene in ZSM-5 (red). Intensities are scaled to correct for different sample sizes.

3.1 Inelastic Neutron Scattering

The collected INS spectra are presented in

Figure 1 (MAPS) and

Figure 2 (TOSCA). The increased resolution of TOSCA at low energies is readily apparent, as are the advantages exhibited by MAPS above ~1200 cm^{-1}. The greatly increased scattering intensity resulting from the increased number of hydrogen scattering centres in the 1-octene containing samples is also clear. Although weak in comparison, the clean ZSM-5 spectrum exhibits features at 3590, 1186-1123, 816 and 457 cm^{-1}. These correspond to the (O-H) stretch of the internal hydroxyl groups and various (O-H) deformations that match the results observed for previous measurements of this catalyst.[20] An additional feature at 308 cm^{-1} is also likely to be an (O-H) deformation and is visible but not assigned in reference 18. The broad peaks below 200 cm^{-1} are the hydrogen motions resulting from various lattice modes. Thus, importantly, INS is providing direct information on the form and nature of the Brønsted acid sites of this class of industrially relevant heterogeneous catalyst.

The vibrational assignment of the peaks in the 1-octene spectra was assisted by computational modelling of the 1-octene system. Multiple potential conformations of 1-octene were optimised through DFT (B3LYP functional, 6-311-G* basis set) and the normal modes of the resulting optimised geometries calculated using GAUSSIAN for

both stages.[30] The calculated normal modes from these models were then used to generate simulated INS spectra using the aCLIMAX software package which were compared with the experimental data from TOSCA.[31] The results providing the closest fit are reproduced in Figure 3, corresponding to the low energy conformer reported by Fraser, et al.[32]: in this conformation the alkyl chain assumes the usual anti-periplanar zig-zag conformation, but the (C=C-C-C) dihedral angle is oriented at ±120º instead of 180º, resulting in the (C=C) bond being staggered out of the plane of the (C-C) bonds.[32] Simulations of conformers where the (C=C) bond is not staggered in this fashion introduce an additional (C=C) torsion mode in the 500 – 600 cm^{-1} region, while those involving a bend in the methylene chain introduce splitting of the peak at 728 cm^{-1}. Since neither of these features is observed in the experimental spectrum it can be accepted that the solid 1-octene is in the conformation shown in the Figure 3 inset.

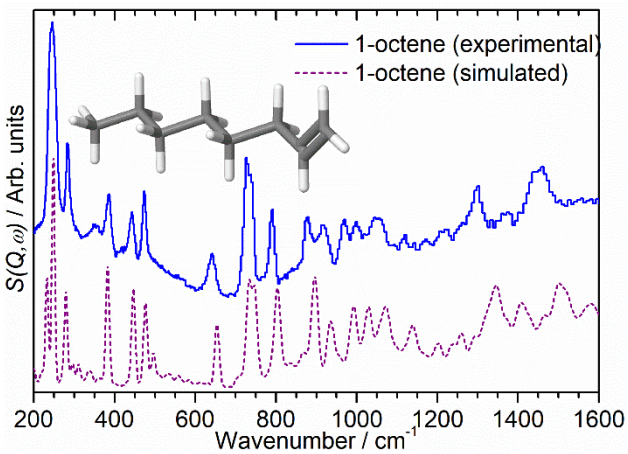

Figure 3: Observed INS spectrum on TOSCA for 1-octene (blue) together with the aCLIMAX-calculated INS spectrum (purple dashed line) for a 1-octene molecule in a partially staggered conformation (*inset*).

The application of these results allows the assignment of the peaks in the 1-octene reference spectra. The slightly broadened peak observed at 1456 cm^{-1} in Figure 2 is

assigned to the overlap of the asymmetric methyl deformation with the two methyl scissors modes, with the narrower peak at 1298 cm^{-1} representing a combination of multiple -CH_2- twisting modes which occur along the axis of the alkyl chain. A smaller peak corresponding to the symmetric methyl deformation is just visible between these peaks at 1371 cm^{-1}. The other peaks of interest are the CH_3 rocking mode at 1118 cm^{-1}, the (C=C) torsion at 639 cm^{-1}, the distinctive peak of the terminal methyl torsion at 245 cm^{-1} and the two transverse acoustic modes located at 167 and 178 cm^{-1}. The alkyl CH_2 rock modes at 728 and 739 cm^{-1} are also of interest since it is known from infrared studies of alkane systems that the frequency of the methylene rocking modes is dependent on the number of consecutive CH_2 groups, *n*, making the position of these peaks a marker for the length of the alkyl chain.[33] In alkanes the frequency is observed to vary from a maximum of 815 cm^{-1} for $n = 1$ to a final value of 722 cm^{-1} for all $n \geq 5$.[33] The fact that the frequency of the 1-octene peak is shifted to a slightly higher value than its chain length would suggest from this series is tentatively attributed to the effect of the adjacent sp^2 carbon on the final methylene group in the chain.

The high energy portion of the MAPS spectrum (
Figure 1) clearly shows the splitting of the 1-octene (C-H) stretch region into a peak at 2884 cm^{-1} with a shoulder at 3046 cm^{-1}. The simplest assignment is to attribute these to the (C-H) stretching modes of the sp^3 and sp^2 carbons respectively, however comparison of the relative peak areas above and below 3000 cm^{-1} show that they do not correspond to the 13:3 ratio expected given the number of hydrogens in each environment. Additionally, this hypothesis fails to account for the additional tail in the peak observed at ~3200 cm^{-1}. Deconvolution of the 2400-3600 cm^{-1} region of the 1-octene spectrum by peak fitting indicates the presence of an additional contribution in

this region caused by the combination of the sp^3 (C-H) stretching modes with the transverse acoustic mode at 178 cm^{-1}. The results of the peak fitting are shown as Figure S1 in the Supporting Information section. Other peaks represent various internal modes and wags and are assigned as detailed in Table 1, with assignments guided by references 33-35 and the DFT calculation described above.

Peak	Frequency (cm^{-1})	Assignment
-	0-150	Multiple overlapping lattice modes
1	167	Transverse acoustic -CH_2- wag
2	178	Transverse acoustic -CH_2- wag
3	245	-CH_3 torsion
4	283	Longitudinal acoustic C-C stretch
5	350	First overtone of peak 1
6	384	Longitudinal acoustic C-C stretch
7	442	Longitudinal acoustic C-C stretch
8	472	C=C-C scissors
9	639	=CH_2 torsion
10	728	-$(CH_2)_n$- in-phase rock, n ≥ 4
11	739	-$(CH_2)_n$- out-of-phase rock, n ≥ 4
12	789	Mixed -(CH_2)- rock/twist
13	875	-CH_3 in-plane rock
14	911	=CH_2 wag
15	967	=CH_2 rock
16	997	=CH- rock
17	1052	-CH_2- twist
18	1118	-CH_3 in-plane rock
19	1217	=CH- rock
20	1298	Multiple -CH_2- twist/wag modes along molecular axis
21	1371	-CH_3 symmetric deformation -CH_2- wag
22	1438	-CH_2- scissors
23	1456	-CH_3 asymmetric deformation -CH_3 scissors
24	2917	sp^3 C-H stretches
25	3071	sp^2 C-H stretches
26	3095	Combination of peaks 2 + 24

Table 1: Vibrational assignments for the INS spectrum of solid 1-octene at <30 K.

On addition of the 1-octene to the zeolite, Figures 1 and 2 show the observed spectrum differs significantly from the spectra of the individual components, indicating chemisorption involving a degree of molecular rearrangement to be occurring. The intensity of the (C-H) stretch region above 3000 cm^{-1} is reduced relative to that observed for pure 1-octene. Peak fitting of this region (Supporting Information, Figure S2) shows the complete elimination of the sp^2 (C-H) stretch component, with the 2400-3600 cm^{-1} region of the ZSM-5/1-octene spectrum only showing contributions from the sp^3 (C-H) stretch modes and their combination with the transverse acoustic mode, which has undergone a reduction in energy and is visible as a shoulder at 143 cm^{-1} in Figure 2. The sp^3 ν(C-H) peak has undergone a minor upward shift of 10 cm^{-1} in the position of the peak maximum, however this is too close to the resolution limit of MAPS at this level of energy transfer to draw meaningful conclusions from this difference. Together with the complete disappearance of the (=CH_2)-associated peaks at 639, 911 and 967 cm^{-1} this indicates that this change involves the carbocation-forming protonation of the octene.[17] This conclusion is further supported by the absence of any peaks corresponding to zeolite (O-H) groups in the loaded spectrum. The lack of an increase in the relative size of the methyl torsion peak supports the assertion by Stepanov, et al.[17] that steric hindrance from the zeolite pores means that adsorbed octene within ZSM-5 is mainly present as a linear secondary carbocation with the normally preferred branched tertiary carbocations forming minority species. Further evidence of this is provided by the presence of the -(CH_2)- rocking modes at 727 cm^{-1} in the combined system; due to the frequency of this mode being dependant on methylene chain length as mentioned above, the fact that it has not shifted significantly

relative to its position in the free 1-octene spectrum indicates that the average methylene chain length in the system remains ≥ 5 adjacent CH_2 units and that the octene is not branching to any significant degree.

Previous literature suggests that 8-carbon molecules like 1-octene are stable species over ZSM-5 at room temperature and although protonation occurs the resulting carbocations do not react further.[17, 21-22] However, the extremely broadened nature of the peaks in the 690-1140 cm^{-1} region (Figure 2) does not appear consistent with the expected results from a simple molecule such as an octene derivative. This was confirmed through DFT modelling of a secondary octene carbocation, which results in a spectrum with peaks at the correct energies but which do not exhibit the necessary broadening to match the experimental spectrum as shown in Figure 4. Expansion of the secondary cation simulation to incorporate contributions from the 14 conformer species which were detected experimentally by Fraser, et al.[32] produces a spectrum which still exhibits individually defined peaks and shows splitting of the 728 cm^{-1} peak due to disruption of the in-phase wag motion in conformers where the methylene chain is bent. Making the assumption that the cation charge has migrated to the third or fourth carbon in the octene chain produces simulated spectra which exhibit fundamental modes in the 600-700 cm^{-1} region which have no experimental counterpart. The results of these further simulations are included as Figure S3 in the Supporting Information section. Taken together, these results indicate that the product species cannot be solely a C_8 carbocation. Further DFT modelling presented in Figure 4 reveals that the experimental spectrum more closely resembles the predicted spectra for longer linear alkanes in the C_{24}-C_{64} range, indicating that the protonated 1-octene does in fact undergo oligomerization to longer chain lengths. The pair of peaks which

are visible in the 788-896 cm^{-1} region of the simulated C_{64} spectrum which does not have an experimental counterpart are due to overtone contributions from the simulation's phonon modes; since the simulation is based on a single molecule which is not constrained by the zeolite micropore the contributions from these modes is overestimated, resulting in the excessive contribution from the overtone peaks in the region reproduced in Figure 4. Based on the lack of evidence for chain branching as detailed above, it appears that the oligomerization proceeds *via* a linear end-to-end polymerization reaction due to restriction by the zeolite pore disfavouring branching reactions. The optimised geometry for all the long-chain alkanes modelled is linear suggesting that the oligomers lie in the straight pore channels.

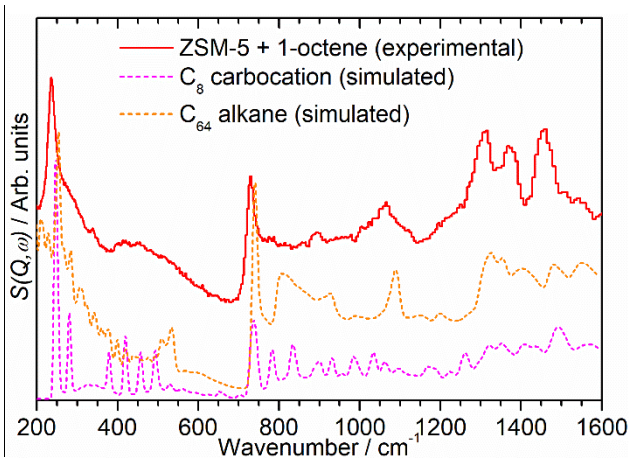

Figure 4: Observed INS spectrum on TOSCA for 1-octene in ZSM-5 (red) together with the aCLIMAX-calculated INS spectra for a secondary octane cation (magenta dashed line) and tetrahexacontane (orange dashed line).

3.2 Quasielastic Neutron Scattering

Visualisation of the QENS spectra of the unloaded zeolite revealed that no significant changes in the width of the elastic peak occur across the temperature range investigated, so any motion of the zeolite cage occurs outside the dynamic window of the spectrometer at these temperatures and the zeolite can be treated as though it is static. In contrast, the spectra of the 1-octene loaded sample exhibit a degree of quasielastic broadening that increases with temperature, indicating that motion is occurring on timescales visible to the OSIRIS spectrometer (~2-50 ps).[28] The positioning of this accessible energy range is such that any motions observed are likely to be due to molecular rotations or the translation of confined hydrocarbon molecules, with any translational movements of internally or externally physisorbed species being too slow to be resolved by this instrument.

For systems undergoing such motion, the shape of the recorded overall scattering function, $S(Q,\omega)$, is given by a combination of an elastic component representing the static scattering species and a quasielastic component representing the mobile species.[36] Due to the extremely large incoherent scattering cross section of hydrogen, the incoherent scattering contribution of other atoms in the system is negligible and the quasielastic scattering function may be taken to be entirely dominated by the uncorrelated motions of hydrogen. The elastic component is a delta function convoluted with an instrument resolution function, which can be provided by a spectrum measured at <10 K where motions are minimal. This will be composed of both incoherent contributions from the static hydrogen atoms and coherent scattering from the zeolite framework. The quasielastic component comprises one or more Lorentzian functions whose broadening describes the motion of the mobile hydrogens.[14, 36] Since the resolution function is provided for the system under investigation by the spectrum

measured at 6 K the contribution from the quasielastic functions may be determined by fitting of the experimental data. The variance of the spectrum with respect to *Q* is complicated by contributions due to coherent Bragg scattering from the zeolite framework and sample environment but, nevertheless, these contributions can be eliminated by subtracting the recorded spectra of the empty zeolite from the loaded spectra at the same temperature leaving just the incoherent scattering contribution from the adsorbed species. This was done and the resulting spectra fitted using the DAVE QENS analysis software suite.[29]

The first fitting was carried out using the resolution function convoluted with a single Lorentzian function; the resulting overall function matched closely in shape but exhibited an offset from the experimental data which was compensated by the addition of a flat background function. This resulted in an overall fit function closely matching the experimental data for all three temperatures studied (273, 323 and 373 K). The single Lorentzian present indicates that the QENS spectra are observing a single motion of mobile hydrogens in the adsorbed species. The existence of a flat background implies an additional motion which falls outside the OSIRIS time window and which is therefore inaccessible to analysis using this data set.

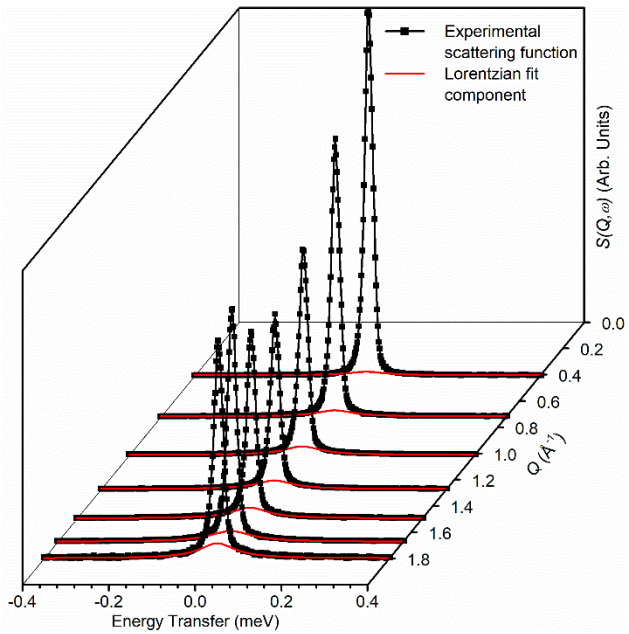

Figure 5: QENS spectra at selected *Q* values for 1-octene in ZSM-5 at 373 K following subtraction of the immobile zeolite contributions (black). The Lorentzian fit component modelling the quasielastic contribution at each *Q* value is also shown (red).

Figure 5 shows the scattering function and the corresponding Lorentzian fit component for the 373 K spectrum at several points across the *Q* range recorded. It is immediately apparent that the Lorentzian function only contributes significantly to the overall scattering function at higher *Q* values: the same pattern is also observed for the spectra at 273 and 323 K. Since *Q* is inversely related to distance,[36] this suggests that the movement of the octene is restricted to localised motions and it does not exhibit the long-range translations reported for linear alkanes in ZSM-5.[15, 37] Localised motions in a QENS spectrum may be characterised by deriving the Elastic Incoherent Structure Factor (EISF, $A_0(Q)$) which is the fraction of the total scattering intensity that is elastic, given by:

$$A_0(Q) = \frac{I_{elastic}(Q)}{I_{elastic}(Q) + I_{quasielastic}(Q)} \quad (1)$$

The quasielastic contribution is always zero at $Q = 0$ giving $A_0(Q) = 1$ and for completely immobile systems this will remain the case at all Q values. Where there is motion, the EISF will initially decrease with increasing Q and the exact shape of the EISF *vs* Q curve is determined by the geometry of motion.[36]

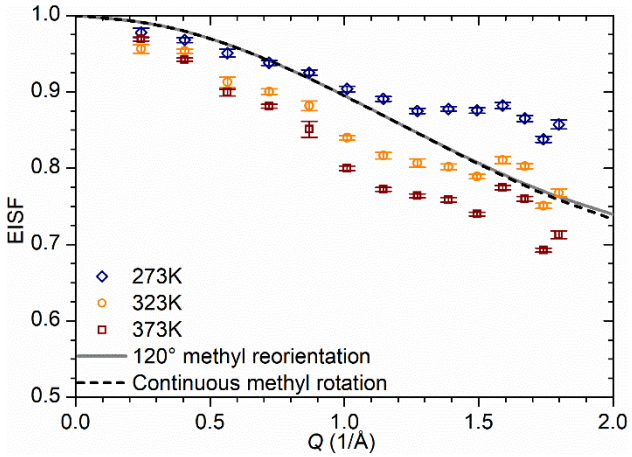

Figure 6: Experimental EISF values for 1-octene in ZSM-5 at 273 K (blue), 323 K (orange) and 373 K (brown) compared to the predicted EISF values for jump (solid black line) and continuous methyl rotation (dashed black line) using the models described in the text.

The EISF values of the loaded zeolite QENS spectra are reproduced in Figure 6 for 273, 323 and 373 K; it can be seen that the overall reduction in EISF magnitude is small at all temperatures and that the motion of the molecules within the zeolite is therefore highly hindered. The fluctuation observed for all three temperatures in the 1.5-1.75 $Å^{-1}$ region is a residual effect of the Bragg peak in that region of Q; expansion of the zeolite structure due to the adsorbed 1-octene results in a shift in the position of the Bragg peaks and results in incomplete cancellation by the baseline subtraction process.

The identification of the exact motion responsible for the quasielastic intensity observed is simplified by the results of the vibrational analysis completed above. Since the hydrocarbon is a long chain constrained within zeolite pores whose diameter is less than the chain length,

only a few types of rotation are physically possible; namely the reorientation of the terminal methyl groups around their C-C bond, either continuously or as a series of 120° jumps between equivalent orientations, or the uniaxial rotation of the entire alkyl chain. Distinguishing between these possibilities can be accomplished through fitting of the EISF curves. Each possible rotation produces a characteristic autocorrelation function for the moving hydrogens that can be converted to an equation for the resulting inelastic neutron scattering law by means of a time Fourier transform.[36] This scattering law can be separated into equations for the elastic and quasielastic contributions which can be used to model the expected EISF values.[14, 36] In the case of a rotation, the generalised scattering law for rotation between *N* equivalent sites on a circle yields the following equation for the EISF:

$$A_0(Q) = \frac{1}{N}\sum_{n=1}^{N} j_o\left[2Qr\sin\left(\frac{\pi n}{N}\right)\right] \qquad (2)$$

where *r* is the radius of rotation, and j_0 is the spherical Bessel function of order zero.[36] In the continuous rotation case the scattering law for true continuous rotation requires knowledge of the angle between the scattering vector and the rotational axis and modelling it is therefore only possible for single crystals. However a sufficiently accurate approximation for powder samples for *Q* values $\leq \pi/r$ may be obtained using Equation (2) provided the value of *N* is sufficiently large.[36]

For the methyl rotations the value of *r* is 1.02 Å, the radius of the circle circumscribed by the methyl hydrogens, which can be calculated from the C-H and C-C bond lengths and angles given by our computational results as shown in Figure S4 in the Supporting Information. Since in both cases the rotation only involves the terminal methyl hydrogens the other hydrogens in the molecule do not contribute to the elastic intensity and it is therefore

necessary to include a correction factor to reflect this. This can be done by splitting the EISF into mobile (*m*) and immobile (*i*) contributions, and weighting each by the proportion in each state ($p_{(i,m)}$ where $p_i + p_m = 1$). The total EISF would then be the sum of each contribution, and since the $A_0(Q)_i$ is always 1:

$$\begin{aligned} A_{0\,eff}(Q) &= p_i A_0(Q)_i \; + \; p_m A_0(Q)_m \\ &= \; p_i \; + \; p_m A_0(Q)_m \end{aligned} \qquad (3)$$

The maximum mobility possible for these rotations will occur with protonation of the adsorbed 1-octene at the terminal carbon but no oligomerization, giving six methyl hydrogens out of seventeen and so $p_m = 0.353$. The predictions from the model for $r = 1.02$ Å and $p_m = 0.353$ are reproduced in Figure 6 as the solid grey line for the jump rotation using $N = 3$ and the broken black line for continuous rotation using $N = 50$; it is apparent that the influence of *N* on the EISF is small at the length scales involved with methyl rotation. It can be seen that both models fail to reach the degree of mobility observed experimentally at 373 K across the *Q* range investigated. Oligomerization of the 1-octene molecules as deduced from the INS data means that the actual proportion of methyl hydrogens in the sample must be lower than the limiting case modelled here, which would result in even higher EISF values than these predictions. The observed elastic intensity therefore cannot be solely due to methyl rotation.

In the case of uniaxial rotation of the alkyl chain, the motion of the CH_2 hydrogens occurs on a circle of 1.40 Å (also shown in Figure S4). Modelling continuous rotation on this radius while assuming that all hydrogens participate, corresponding to the limiting case of a chain of infinite length, produces the EISF plot shown as the black line in Figure 7: it can be seen that in this case the maximum mobility case predicts lower-than-observed EISF values across

the *Q* range. Close fits for the experimental data can be obtained by assuming partial sample immobility and fitting the model to the experimental data with respect to p_m, shown as the broken lines in Figure 7: the final p_m values used to generate these fits are reproduced in Table 2 and indicate that the mobile fraction of the hydrogens is temperature dependant, varying from 18.0 % at 273 K to 35.8 % at 373 K. This degree of immobility is too high to be entirely due to non-participation by the terminal hydrogens in the alkyl chain and indicates that a majority of the oligomers remain completely immobile at these temperatures. This high degree of immobility is likely due to strong hydrocarbon-zeolite interactions due to the short distances between the methylene hydrogens and the pore walls in the zeolite channels. Experimental adsorption enthalpies as high as – 79 kJ/mol have been reported for short-chain (C_6) alkanes in zeolite, with computational studies indicating that the effect of hydrogen bonding will lead to even stronger interactions in H-ZSM5.[38-39] Given these high energies, it is possible that at the temperatures investigated the mobile fraction represents those oligomers which terminate within a pore intersection and therefore have a proportion of the chain which is further from the zeolite pore walls, reducing the overall binding energy which hinders the rotation. Increased temperatures result in a more tightly bound portion of the oligomers, residing within the pore channels, gaining sufficient energy to break the framework-sorbate interactions and participate in rotational movement. Since the temperature range investigated does not reach a point where all CH_2 groups are participating in the rotation and p_m attains a plateau value, it is therefore not possible to use p_m to estimate the average chain length in the sample. While the alteration of the shape of the EISF plot due to the large scaling factor from the low p_m means that the possibility of secondary contributions from methyl rotations to the overall shape cannot be ruled out with complete certainty (as changes to the plot shape due to the

addition of a 3-site rotational model would be too insignificant to be noticeable due to the p_m scaling), the close fit of the uniaxial rotation model to the experimental data indicates that it is responsible for the majority of this quasielastic character and the contributions of other modes are likely to be negligible.

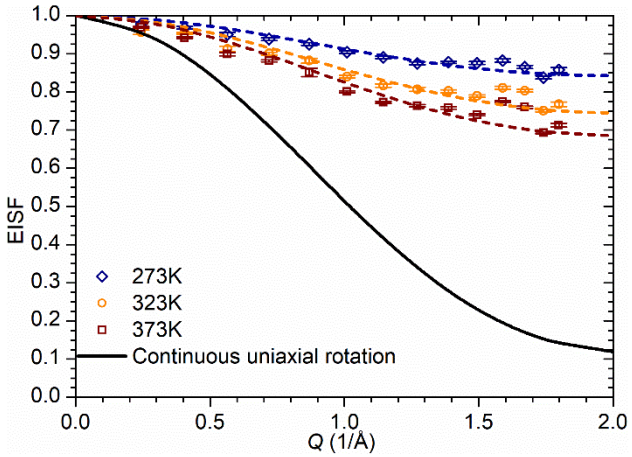

Figure 7: Experimental EISF values for 1-octene in ZSM-5 at 273 K (blue), 323 K (orange) and 373 K (brown). The solid black line represents the calculated EISF resulting from continuous uniaxial rotation of the alkyl chain, assuming all hydrogens participate. The dotted lines represent the results of a partially-immobile modification of this rotation as described in the text using the p_m values in Table 2.

A property of continuous rotations of this form is that the degree of quasielastic broadening remains constant with respect to Q and that the half-width at half-maximum (HWHM, Γ) of the Lorentzian corresponds to the inverse of the time constant of the rotation (τ) and therefore is the same as the rotational constant (D_r).

$$D_r = \frac{1}{\tau} = \Gamma \qquad (4)$$

Figure 8 shows that this Q-independent relationship holds true at all three temperatures within the limits of experimental accuracy and allows the extraction of D_r values for the

rotation at each temperature, reproduced in Table 2. Over the temperature range studied, these values follow an Arrhenius relationship, leading to a calculated activation energy for the rotation of 5.1 kJ mol^{-1}. This is approximately 27% of the activation energy previously reported for similar oligomer motions in bulk polyethylene.[40] We consider that that the reduction in activation energy is due to the isolated nature of the oligomer chains within the zeolite, with pore wall-oligomer interactions offering a lower barrier to rotation than chain-chain interactions, particularly when the population of oligomers in the pore intersections is considered.

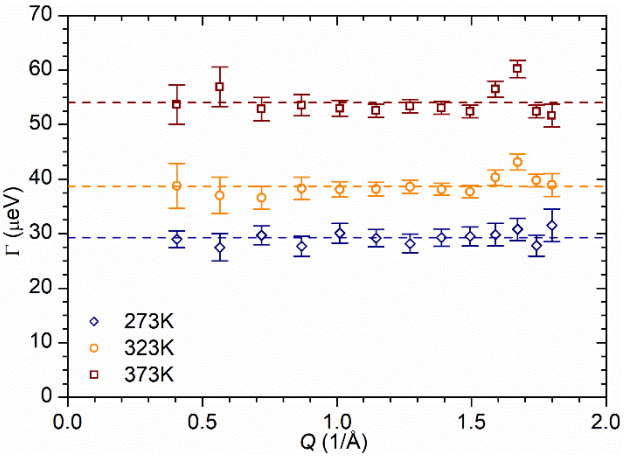

Figure 8: Lorentzian HWHM vs *Q* plots for 1-octene in ZSM-5 at 273 (blue), 323 (orange) and 373 K (brown). Dotted lines represent linear fits to the data used to derive the HWHM values reported in Table 2.

Table 2: Summary of dynamical parameters derived from QENS data fitting for the combined ZSM-5 / 1-octene system.

***T* (K)**	p_m	***Γ* (μeV)**	D_r **(s^{-1})**
273	0.180	29.3	4.45×10^{10}
323	0.291	38.7	5.89×10^{10}
373	0.358	54.0	8.21×10^{10}

From these combined results it appears that the 1-octene / ZSM-5 system consists of long-chain linear hydrocarbons formed by the catalytic oligomerization of the 1-octene, as observed in the INS spectrum, which are large enough to be immobilised within the zeolite pores. A temperature-dependant fraction of the oligomers are able to break the forces holding them to the pore wall sufficiently to undergo localised rotation; the fact that this rotation is either partially or completely due to free rotation of the alkyl chain around its long axis implies that the mobile hydrocarbons are located along the length of the straight pore channels in the zeolite.

4. Conclusions

The properties and dynamics of 1-octene adsorbed in ZSM-5 at 293 K have been investigated *via* INS and QENS. The inelastic results are in close agreement with predicted spectra from DFT simulations and match predictions derived from literature reports of INS investigations of related alkene and alkane species,[34-35] and general trends observed for vibrational spectroscopy of alkyl chains.[33] Moreover, the INS data together with the complete absence of translational mobility visible on QENS timescales indicates that the oligomerization reaction proceeds to completion on addition to the activated zeolite even at 293 K. Steric hindrance by the zeolite pore structure means that oligomerization proceeds *via* an end-to-end mechanism to give linear products. Chain growth proceeds until the size of the molecule renders it immobile within the pore channel in terms of long range movement: mobility in the form of localised rotations of the alkyl chain is still possible and observed for chains located in the straight pore channels with rotational constants in the range 4.48–8.21 × 10^{10} s^{-1}. The

percentage of mobile hydrocarbon increases with temperature (Table 2), while the presence of movement on QENS timescales (ps) supports the identification of the sorbate as a carbocation rather than a bonded silyl ether. The ability of the INS technique to provide information on the hydrocarbon-zeolite interaction in FCC catalysts means that it can provide valuable insight both in explaining the results of QENS-derived dynamical measurements and in investigating the role played by structural changes in the zeolite in affecting the cracking reaction. Thus, this study provides an awareness of how a reagent such as 1-octene chemisorbs and interacts with an activated ZSM-5 catalyst. This then provides a platform where reagent/product interactions can be further investigated as a function of certain catalyst pre-treatments, *e.g.* the examination of ZSM-5 catalyst samples that have experienced steaming regimes that mimic the FCC industrial scenario. The latter activity presently represents 'work in progress'.

Conflicts of interest

There are no conflicts of interest to declare.

Acknowledgements Johnson Matthey plc and the EPSRC are thanked for postgraduate student support (APH, AZ) via the Industrial CASE scheme. Johnson Matthey plc is additionally thanked for provision of the ZSM-5 catalyst. A.J.OM acknowledges the Ramsay Memorial Trust for the provision of a Ramsay Memorial Fellowship. The Science and Technology Facilities Council is thanked for the provision of neutron beamtime. The resources and support provided by the UK Catalysis Hub *via* membership of the UK Catalysis Hub consortium and funded by EPSRC (grants EP/K014706/1, EP/K014668/1,

EP/K014854/1, EP/K014714/1 and EP/M013219/1) is gratefully acknowledged. Daniel Dervin (Queens University Belfast) is thanked for useful discussions on the principles of QENS analysis.

Supporting Information

Figure S1, showing the fitted curves for deconvolution of the (C-H) stretch region of the INS spectrum of 1-octene into its component modes; Figure S2, showing the fitted curves for deconvolution of the (C-H) stretch region of the INS spectrum of 1-octene exposed to activated ZSM-5 at 293 K into its component modes; Figure S3, comparing the measured INS spectrum for 1-octene exposed to activated ZSM-5 at 293 K with a number of octene carbocations; Figure S4, showing trigonometric derivations of the radii of rotation for the CH_3 and CH_2 hydrogens in an alkyl chain.

References

1. Degnan, T. F.; Chitnis, G. K.; Schipper, P. H., History of ZSM-5 fluid catalytic cracking additive development at Mobil. *Microporous Mesoporous Mat.* **2000,** *35-6*, 245-252.
2. den Hollander, M. A.; Wissink, M.; Makkee, M.; Moulijn, J. A., Gasoline conversion: reactivity towards cracking with equilibrated FCC and ZSM-5 catalysts. *Appl. Catal., A* **2002,** *223* (1-2), 85-102.
3. den Hollander, M. A.; Wissink, M.; Makkee, M.; Moulijn, J. A., Synergy effects of ZSM-5 addition in fluid catalytic cracking of hydrotreated flashed distillate. *Appl. Catal., A* **2002,** *223* (1-2), 103-119.

4. Akah, A.; Al-Ghrami, M., Maximizing propylene production via FCC technology. *Appl. Petrochem. Res.* **2015,** *5* (4), 377-392.

5. Sadrameli, S. M., Thermal/catalytic cracking of liquid hydrocarbons for the production of olefins: A state-of-the-art review II: Catalytic cracking review. *Fuel* **2016,** *173*, 285-297.

6. Awayssa, O.; Al-Yassir, N.; Aitani, A.; Al-Khattaf, S., Modified HZSM-5 as FCC additive for enhancing light olefins yield from catalytic cracking of VGO. *Appl. Catal., A* **2014,** *477*, 172-183.

7. Thomas, C. L., Chemistry of Cracking Catalysts. *Ind. Eng. Chem.* **1949,** *41* (11), 2564-2573.

8. Olson, D. H.; Kokotailo, G. T.; Lawton, S. L.; Meier, W. M., Crystal-structure and structure-related properties of ZSM-5. *J. Phys. Chem.* **1981,** *85* (15), 2238-2243.

9. Guo, Y. H.; Pu, M.; Wu, J. Y.; Zhang, J. Y.; Chen, B. H., Theoretical study of the cracking mechanisms of linear alpha-olefins catalyzed by zeolites. *Appl. Surf. Sci.* **2007,** *254* (2), 604-609.

10. Guerzoni, F. N.; Abbot, J., Cracking of an industrial feedstock over combinations of H-ZSM-5 and HY - the influence of H-ZSM-5 pretreatment. *Appl. Catal., A* **1994,** *120* (1), 55-69.

11. Triantafyllidis, K. S.; Vlessidis, A. G.; Nalbandian, L.; Evmiridis, N. P., Effect of the degree and type of the dealumination method on the structural, compositional and acidic characteristics of H-ZSM-5 zeolites. *Microporous Mesoporous Mat.* **2001,** *47* (2-3), 369-388.

12. O'Malley, A. J.; Catlow, C. R. A., Chapter 6 - Sorbate Dynamics in Zeolite Catalysts. In *Experimental Methods in the Physical Sciences*, Fernandez-Alonso, F.; Price, D. L., Eds. Academic Press: 2017; Vol. 49, pp 349-401.

13. O'Malley, A. J.; Parker, S. F.; Catlow, C. R. A., Neutron spectroscopy as a tool in catalytic science. *Chem. Commun.* **2017,** *53* (90), 12164-12176.

14. Jobic, H.; Theodorou, D. N., Quasi-elastic neutron scattering and molecular dynamics simulation as complementary techniques for studying diffusion in zeolites. *Microporous Mesoporous Mat.* **2007,** *102* (1-3), 21-50.

15. Jobic, H., Diffusion of linear and branched alkanes in ZSM-5. A quasi-elastic neutron scattering study. *J. Mol. Catal. A: Chem.* **2000,** *158* (1), 135-142.

16. Potter, M. E.; O'Malley, A. J.; Chapman, S.; Kezina, J.; Newland, S. H.; Silverwood, I. P.; Mukhopadhyay, S.; Carravetta, M.; Mezza, T. M.; Parker, S. F.*, et al.*, Understanding the Role of Molecular Diffusion and Catalytic Selectivity in Liquid-Phase Beckmann Rearrangement. *ACS Catal.* **2017,** *7* (4), 2926-2934.

17. Stepanov, A. G.; Luzgin, M. V.; Romannikov, V. N.; Zamaraev, K. I., Carbenium ion properties of octene-1 adsorbed on zeolite H-ZSM-5. *Catal. Lett.* **1994,** *24* (3), 271-284.

18. Parker, S. F.; Lennon, D.; Albers, P. W., Vibrational Spectroscopy with Neutrons: A Review of New Directions. *Appl. Spectrosc.* **2011,** *65* (12), 1325-1341.

19. Howe, R. F.; McGregor, J.; Parker, S. F.; Collier, P.; Lennon, D., Application of Inelastic Neutron Scattering to the Methanol-to-Gasoline Reaction Over a ZSM-5 Catalyst. *Catal. Lett.* **2016,** *146* (7), 1242-1248.

20. Suwardiyanto; Howe, R. F.; Gibson, E. K.; Catlow, C. R. A.; Hameed, A.; McGregor, J.; Collier, P.; Parker, S. F.; Lennon, D., An assessment of hydrocarbon species in the methanol-to-hydrocarbon reaction over a ZSM-5 catalyst. *Faraday Discuss.* **2017,** *197*, 447-471.

21. Ghosh, A. K.; Kydd, R. A., A Fourier-transform infrared spectral study of propene reactions on acidic zeolites. *J. Catal.* **1986,** *100* (1), 185-195.

22. Spoto, G.; Bordiga, S.; Ricchiardi, G.; Scarano, D.; Zecchina, A.; Borello, E., IR study of ethene and propene oligomerization on H-ZSM-5: hydrogen-bonded precursor formation, initiation and propagation mechanisms and structure of the entrapped oligomers. *J. Chem. Soc., Faraday Trans.* **1994,** *90* (18), 2827-2835.

23. Warringham, R.; Bellaire, D.; Parker, S. F.; Taylor, J.; Ewings, R. A.; Goodway, C. M.; Kibble, M.; Wakefield, S. R.; Jura, M.; Dudman, M. P.*, et al.*, Sample environment issues relevant to the acquisition of inelastic neutron scattering measurements of heterogeneous catalyst samples. *J. Phys.: Conf. Ser.* **2014,** *554* (1), 012005.

24. Parker, S. F.; Fernandez-Alonso, F.; Ramirez-Cuesta, A. J.; Tomkinson, J.; Rudic, S.; Pinna, R. S.; Gorini, G.; Castañon, J. F., Recent and future developments on TOSCA at ISIS. *J. Phys.: Conf. Ser.* **2014,** *554* (1), 012003.

25. Arnold, O.; Bilheux, J. C.; Borreguero, J. M.; Buts, A.; Campbell, S. I.; Chapon, L.; Doucet, M.; Draper, N.; Ferraz Leal, R.; Gigg, M. A.*, et al.*, Mantid—Data analysis and visualization package for neutron scattering and SR experiments. *Nucl. Instrum. Methods Phys. Res., Sect. A* **2014,** *764*, 156-166.

26. Mslice. http://mslice.isis.rl.ac.uk/Main_Page (accessed June 2018).

27. Silverwood, I. P.; Sakai, V. G., Propane diffusion in ZSM-5 pores measured by quasielastic neutron scattering under macroscopic flow. *Chem. Eng. Sci.* **2018,** *186*, 116-121.

28. Telling, M. T. F.; Andersen, K. H., Spectroscopic characteristics of the OSIRIS near-backscattering crystal analyser spectrometer on the ISIS pulsed neutron source. *Phys. Chem. Chem. Phys.* **2005,** *7* (6), 1255-1261.

29. Azuah, R. T.; Kneller, L. R.; Qiu, Y. M.; Tregenna-Piggott, P. L. W.; Brown, C. M.; Copley, J. R. D.; Dimeo, R. M., DAVE: A Comprehensive Software Suite for the Reduction, Visualization, and Analysis of Low Energy Neutron Spectroscopic Data. *J. Res. Natl. Inst. Stand. Technol.* **2009,** *114* (6), 341-358.

30. Frisch, M. J.; Trucks, G. W.; Schlegel, H. B.; Scuseria, G. E.; Robb, M. A.; Cheeseman, J. R.; Montgomery, J., J. A.; Vreven, T.; Kudin, K. N.; Burant, J. C.*, et al. Gaussian 03W*, Version 6.0; Gaussian Inc.: Wallingford CT, United States, 2004.

31. Ramirez-Cuesta, A. J., aCLIMAX 4.0.1, The new version of the software for analyzing and interpreting INS spectra. *Comput. Phys. Commun.* **2004,** *157* (3), 226-238.

32. Fraser, G. T.; Suenram, R. D.; Lugez, C. L., Investigation of conformationally rich molecules: Rotational spectra of fifteen conformational isomers of 1-octene. *J. Phys. Chem. A* **2001,** *105* (43), 9859-9864.

33. Bower, D. I.; Maddams, W. F., *The Vibrational Spectroscopy of Polymers*. Cambridge University Press: Cambridge, 1989, DOI: 10.1017/CBO9780511623189.

34. Braden, D. A.; Parker, S. F.; Tomkinson, J.; Hudson, B. S., Inelastic neutron scattering spectra of the longitudinal acoustic modes of the normal alkanes from pentane to pentacosane. *J. Chem. Phys.* **1999,** *111* (1), 429-437.

35. Lennon, D.; McNamara, J.; Phillips, J. R.; Ibberson, R. M.; Parker, S. F., An inelastic neutron scattering spectroscopic investigation of the adsorption of ethene and propene on carbon. *Phys. Chem. Chem. Phys.* **2000,** *2* (19), 4447-4451.

36. Bee, M., *Quasielastic Neutron Scattering: Principles and Applications in Solid State Chemistry, Biology and Materials Science*. Adam Hilger: Bristol and Philadelphia, 1988.

37. O'Malley, A. J.; Catlow, C. R. A., Molecular dynamics simulations of longer n-alkanes in silicalite: state-of-the-art models achieving close agreement with experiment. *Phys. Chem. Chem. Phys.* **2015,** *17* (3), 1943-1948.

38. Eder, F.; Lercher, J. A., On the role of the pore size and tortuosity for sorption of alkanes in molecular sieves. *J. Phys. Chem. B* **1997,** *101* (8), 1273-1278.

39. Chiu, C. C.; Vayssilov, G. N.; Genest, A.; Borgna, A.; Rosch, N., Predicting Adsorption Enthalpies on Silicalite and HZSM-5: A Benchmark Study on DFT Strategies Addressing Dispersion Interactions. *J. Comput. Chem.* **2014,** *35* (10), 809-819.

40. Peterlin-Neumaier, T.; Springer, T., Investigation of relaxation processes in linear polyethylene in the 10^{-9} sec region by means of high-resolution neutron spectroscopy. *J. Polym. Sci., Polym. Phys. Ed.* **1976,** *14* (8), 1351-1359.

Supporting Information

Investigation Of The Dynamics Of 1-Octene Adsorption At 293 K In A ZSM-5 Catalyst By Inelastic And Quasielastic Neutron Scattering

Alexander P. Hawkins [a,b], Alexander J. O'Malley [b,c], Andrea Zachariou [a,b], Paul Collier [d], Russell A. Ewings [e], Ian P. Silverwood [e], Russell F. Howe [f], Stewart F. Parker [b,e], and David Lennon [a,b]*

[a] School of Chemistry, Joseph Black Building, University of Glasgow, Glasgow G12 8QQ, UK

[b] UK Catalysis Hub, Research Complex at Harwell, STFC Rutherford Appleton Laboratory, Chilton, Oxon OX11 0FA, UK

[c] Cardiff Catalysis Institute, School of Chemistry, Cardiff University, Main Building, Cardiff, CF10 3AT, UK.

[d] Johnson Matthey Technology Centre, Blounts Court, Sonning Common, Reading RG4 9NH, UK

[e] ISIS Facility, STFC Rutherford Appleton Laboratory, Chilton, Oxon OX11 0QX, UK

[f] Department of Chemistry, University of Aberdeen, Aberdeen, AB24 3UE, UK

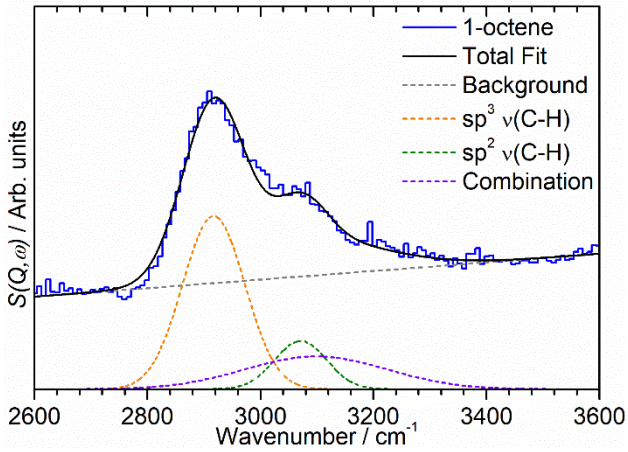

Figure S1: 2600-3600 cm^{-1} region of the INS spectrum on MAPS for 1-octene (blue) showing the (C-H) stretching bands and the results of peak fitting analysis to deconvolute them into separate modes. This analysis identifies contributions from (C-H) stretches involving sp^3 carbon centres (orange dashed line), sp^2 carbon (C-H) stretches (green dashed line) and modes involving the simultaneous excitement of a sp^3 (C-H) stretch and the methylene transverse acoustic mode located at 178 cm^{-1} (purple dashed line). The non-flat baseline (grey dashed line) is due to the effect of noise from multiple scattering in the dense 1-octene sample as the energy approaches the incident neutron energy used for this measurement (5244 cm^{-1}).

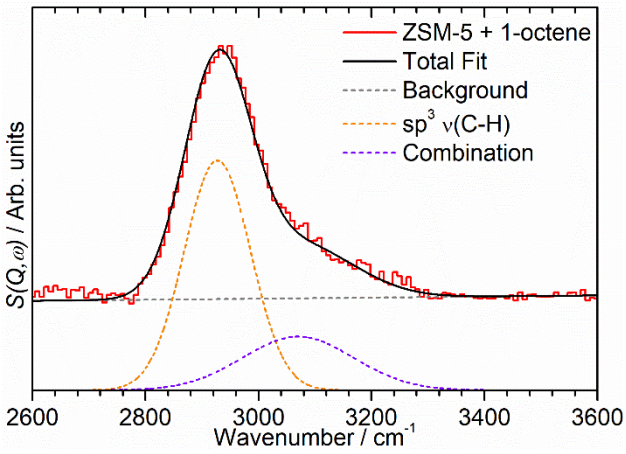

Figure S2: 2600-3600 cm^{-1} region of the INS spectrum on MAPS for 1-octene in ZSM-5 (red) showing the (C-H) stretching bands and the results of peak fitting analysis to deconvolute them into separate modes. This analysis identifies contributions from (C-H) stretches involving sp^3 carbon centres (orange dashed line) and modes involving the simultaneous excitement of a sp^3 (C-H) stretch and the methylene transverse acoustic mode located at 143 cm^{-1} (purple dashed line). No vibrations involving sp^2 carbons are visible at this resolution.

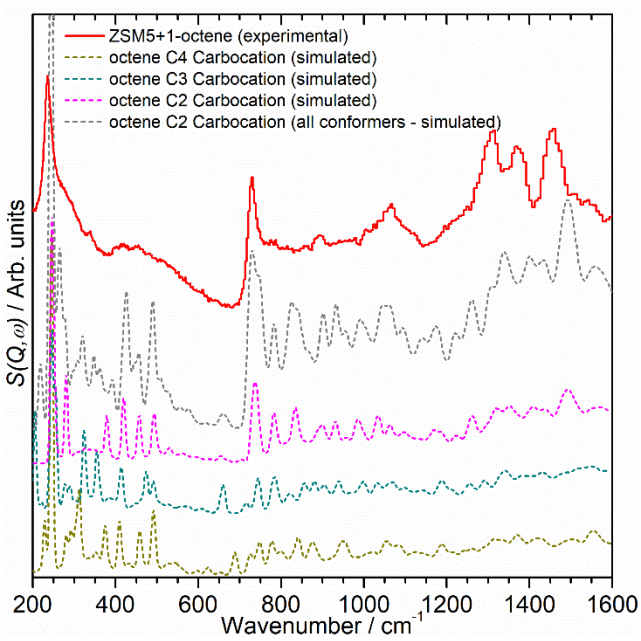

Figure S3: Observed INS spectrum on TOSCA for 1-octene in ZSM-5 together with the aCLIMAX-calculated spectra for a number of alternative C_8 species to those presented in Figure 4, showing that none of these species provide a close match to the experimental spectrum. The 'all conformers' simulation is derived by modelling all 14 experimentally observed conformers reported by Fraser, et al. [32] and combining the resulting spectra.

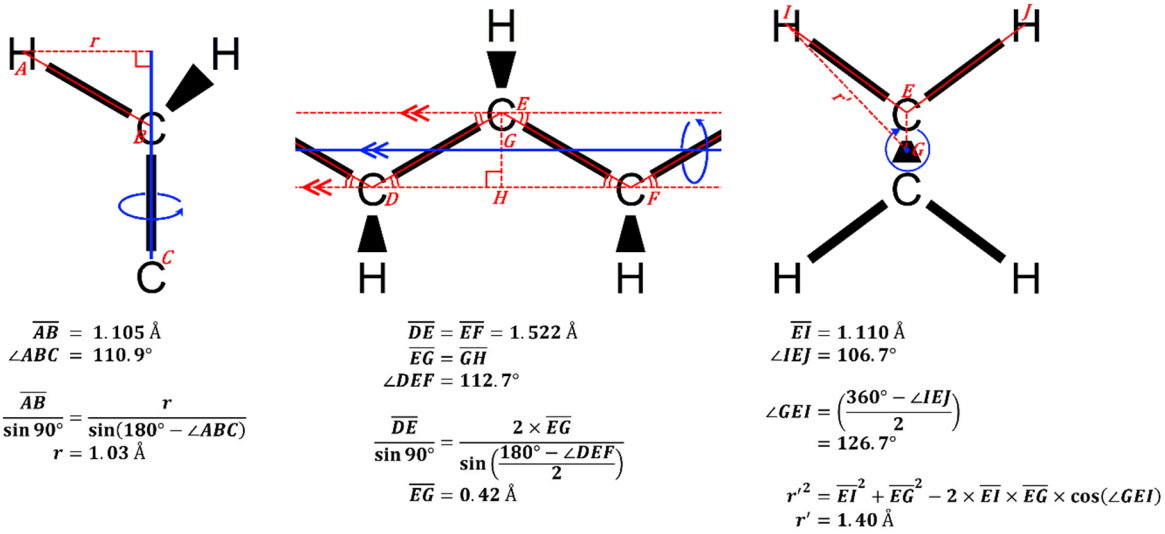

$$\overline{AB} = 1.105\ \text{Å}$$
$$\angle ABC = 110.9°$$
$$\frac{\overline{AB}}{\sin 90°} = \frac{r}{\sin(180° - \angle ABC)}$$
$$r = 1.03\ \text{Å}$$

$$\overline{DE} = \overline{EF} = 1.522\ \text{Å}$$
$$\overline{EG} = \overline{GH}$$
$$\angle DEF = 112.7°$$
$$\frac{\overline{DE}}{\sin 90°} = \frac{2 \times \overline{EG}}{\sin\left(\frac{180° - \angle DEF}{2}\right)}$$
$$\overline{EG} = 0.42\ \text{Å}$$

$$\overline{EI} = 1.110\ \text{Å}$$
$$\angle IEJ = 106.7°$$
$$\angle GEI = \left(\frac{360° - \angle IEJ}{2}\right) = 126.7°$$
$$r'^2 = \overline{EI}^2 + \overline{EG}^2 - 2 \times \overline{EI} \times \overline{EG} \times \cos(\angle GEI)$$
$$r' = 1.40\ \text{Å}$$

Figure S4: Trigonometric derivations of the radii of rotation for the CH_3 and CH_2 hydrogens in an alkyl chain from bond lengths and angles obtained from DFT structural optimisations.

Reference

32. G.T. Fraser et al., *J. Phys. Chem. A*, 105 (2001) 9859.